Journal of Science Research International (JSRI)
ISSN: 2456-6365 (Online)

OPEN ACCESS

SYNTHESIS AND CHARACTERIZATION OF COBALT FERRITE–SUPPORTED WASTE FOUNDRY SAND (CO-FE_2O_4/WFS) FOR DYE DEGRADATION

Tejeswini T. Mangale, Mayuri A. Lad, Suraj S. Desai,

Uttam B. Chougale and Chandrashekhar R. Patil*

PG Department of Chemistry,

Karmaveer Hire Arts, Science, Commerce and Education College, Gargoti, Maharashtra, India 416 209

**Corresponding author E-mail: patil.shekhar69@gmail.com*

Received: 17 January 2025	Revised: 03 March 2026	Accepted: 19 March 2026	Published: 30 March 2026

DOI: **https://doi.org/10.5281/zenodo.19335858**

Abstract:

In this work, we propose and assess a hybrid photocatalyst based on waste foundry sand (WFS), a common industrial by-product, supported by cobalt ferrite ($CoFe_2O_4$). While $CoFe_2O_4$ offers photocatalytic activity driven by visible light, the WFS serves as both an adsorbent and a structural support XRD, SEM, and FTIR analyses were used to characterize the composite ($CoFe_2O_4$/WFS), which was created utilizing an in-situ co-precipitation approach. By adjusting pH, catalyst dose, contact time, and starting dye concentration, the photocatalytic degradation of MB under visible light irradiation was examined.

Keywords: *Cobalt Ferrite Nanoparticles, Waste Foundry Sand, Co-Precipitation, Photocatalytic Activity.*

1. Introduction

The textile, leather, printing, paper, and plastic sectors all make extensive use of synthetic dyes, which are produced in excess of 800,000 tons annually worldwide. A significant portion finds its way into industrial effluents untreated, posing serious ecological risks, contaminating groundwater, and reducing sunlight penetration. A common cationic dye, methylene blue (MB), is not biodegradable, carcinogenic at high concentrations, and produces harmful byproducts when exposed to sunlight.

Aquatic habitats are seriously threatened by industrial discharge of synthetic dyes, especially Methylene Blue (MB), because of their high stability, toxicity, and resistance to biodegradation. Conventional adsorption techniques with inexpensive materials frequently have problems with regeneration and incomplete mineralization.

Instead of breaking down pollutants, conventional treatment methods (adsorption, coagulation, bacterial or fungal degradation, membrane filtration) frequently move them to another phase. Complete mineralization of

organic contaminants is a benefit of Advanced Oxidation Processes (AOPs), especially visible-light-driven photocatalysis.

When compared to individual components, the composite's synergistic adsorption–photocatalysis action resulted in noticeably greater MB elimination. According to mechanistic research, superoxide and hydroxyl radicals are primarily responsible for MB breakdown. The WFS–$CoFe_2O3$ composite exhibits outstanding structural stability and is magnetically recoverable and reusable. The findings imply that this inexpensive photocatalyst made from garbage presents a viable method for treating wastewater in a sustainable manner.

1.1. Cobalt ferrite as a photocatalyst

Cobalt ferrite ($CoFe_2O_4$) is a spinel ferrite semiconductor with:

- Narrow bandgap (~1.8–2.2 ev),
- High thermal and chemical stability,
- Magnetic recoverability,
- High absorption in the visible region,
- Robust generation of reactive oxygen species (ROS).

Although $CoFe_2O_3$ nanoparticles are effective photocatalysts, they tend to aggregate, reducing active surface area.

1.2. Waste Foundry Sand (WFS) as a support material

WFS is an industrial waste containing mainly quartz, silica, clay, and minor metal oxides. It is:

- Abundant and low-cost,
- Thermally stable,
- Moderately porous,
- Suitable for adsorption of dyes and metals.

2. Materials and Methods

2.1. Materials

- Waste foundry sand (collected from local foundry industry).
- Cobalt nitrate hexahydrate [$Co(NO_3)_2 \cdot 6H_2O$].
- Ferric nitrate nonahydrate [$Fe(NO_3)_3 \cdot 9H_2O$].
- Sodium hydroxide (NaOH).
- Methylene Blue (analytical grade).

2.2. Pre-treatment of waste foundry sand

WFS were frequently cleaned with deionized water to get rid of organics, dust, and clay lumps. After that, dry for 12 hours at 105°C. Lastly, to improve porosity and eliminate any remaining organics, it was calcined for three hours at 600°C.

2.3. Synthesis of $CoFe_2O_4$ nanoparticles

$CoFe_2O_4$ composite were synthesized via co-precipitation:

In water, stoichiometric precursors (Co^{2+}: Fe^{3+} = 1:2) were dissolved. Then, drop by drop, NaOH (2 M) was added to keep the pH at 11. Two hours were spent heating the mixture to 80°C. The black precipitate that resulted was cleaned, dried, and then calcined at 500°C.

2.4. Fabrication of $CoFe_2O_4$/ WFS composite

- Pre-treated WFS was dispersed in water and ultrasonicated.
- Co^{2+}/Fe^{3+} precursors were introduced into the WFS suspension.
- NaOH was added to precipitate $CoFe_2O_4$ directly onto the WFS surface.
- Composite was washed and dried at 100°C.
- Mild calcination at 300°C ensured nanoparticle binding.

3. Results and Discussion

3.1. XRD analysis

Figure 1 displays the cobalt ferrite CoFe2O4/WFS XRD patterns. A single-phase spinel structure with a little fraction of α-Fe2O3 included all of the peaks. The XRD pattern was analyzed using X-Powder Software, and crystalline phases were found. The spectrum of cobalt ferrites (CoFe2O4)-WFS composites revealed peaks at 2θ (23.48, 30.12, 35.46, 36.74, 43.07, 53.49, 56.81, 63.03), which demonstrate the ferrite's spinel cubic structure.

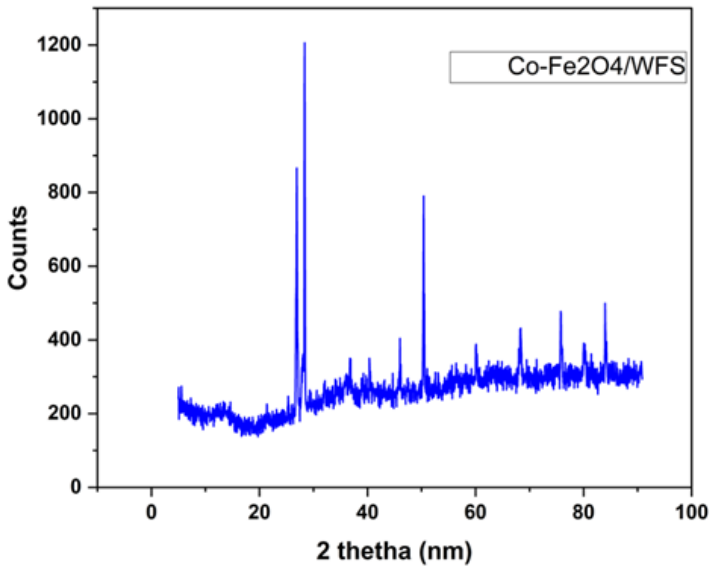

Figure 1: XRD spectrum of $CoFe_2O_4$/WFS

3.2. SEM analysis

- WFS showed irregular sand grains with smooth texture.
- $CoFe_2O_4$ appeared as dark clusters on WFS surfaces.

Nanoparticles formed a uniform coating, increasing available surface sites.

3.3. FTIR spectra

Figure 3 displays the cobalt ferrite FTIR spectrum. Co-O vibrations when Co ions were in a tetrahedral position were identified as the cause of the frequency band at 787.72 cm−1 in the cobalt ferrite/WFS FTIR spectra. The band at 906.97 cm−1 is associated with water hydration by CoOOH. The CoFe2O4 system was characterized by the band at 1058.46 cm−1 and 1196.95 cm−1, which was caused by residual Fe-OOH. Si–O–Si stretching at about 1080 cm^{-1} (WFS). Typical spinel ferrite bands at 580–430 cm^{-1} include Co–O and Fe–O.The contact between the ferrite nanoparticles and the WFS surface was evidenced by a decrease in the strength of the Si–OH signal.

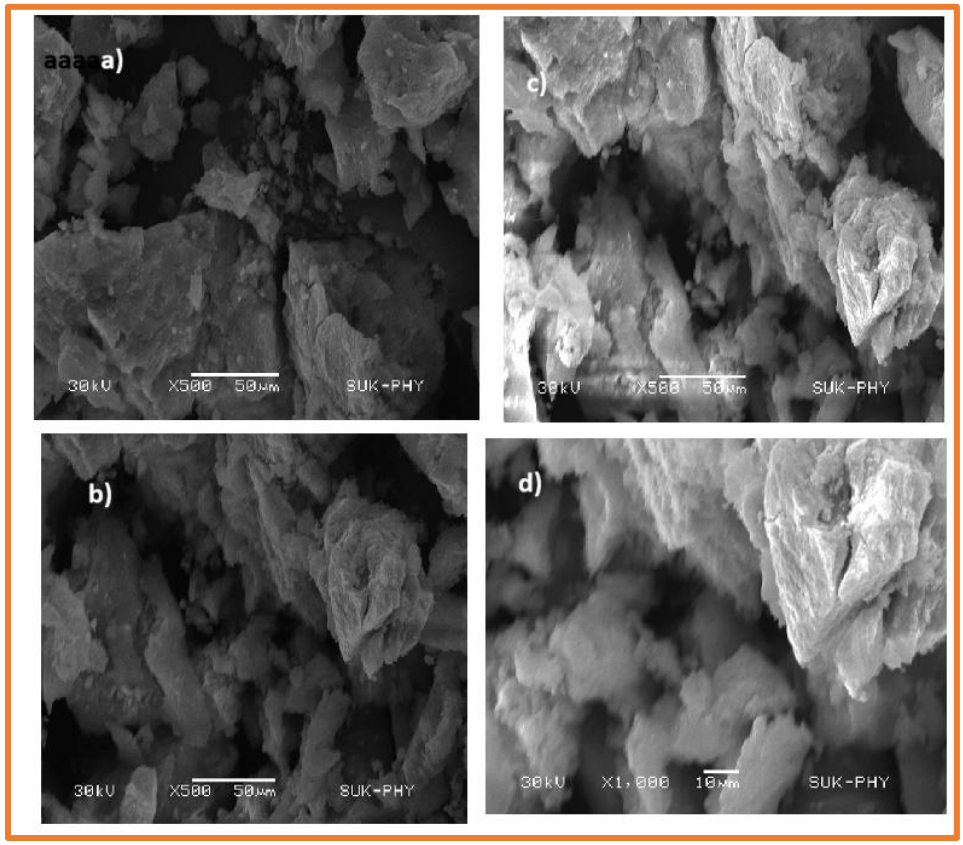

Figure 2: SEM image of $CoFe_2O_4$/WFS

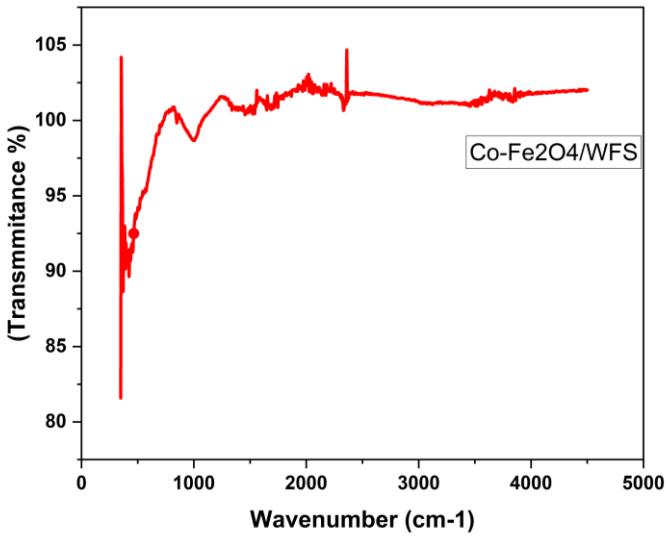

Figure 3: FTIR spectra of $CoFe_2O_4$/WFS

3.4. Photocatalytic degradation of MB

3.4.1. Preparation of MB solution

- Stock solution: 1000 mg/L MB.
- Working concentrations: 5–25 mg/L.

3.4.2. Photocatalytic experiment

- 100 mL of MB solution placed in a quartz reactor.
- Catalyst dose varied from 0.1–0.5 g/L.
- Stirred in the dark for 30 min to establish adsorption equilibrium.
- Exposed to visible light (LED/halogen lamp ~150 W).
- Samples withdrawn at intervals, centrifuged, and analyzed at 663 nm.

3.4.1. Optimization of different variables affecting degradation of MB dye

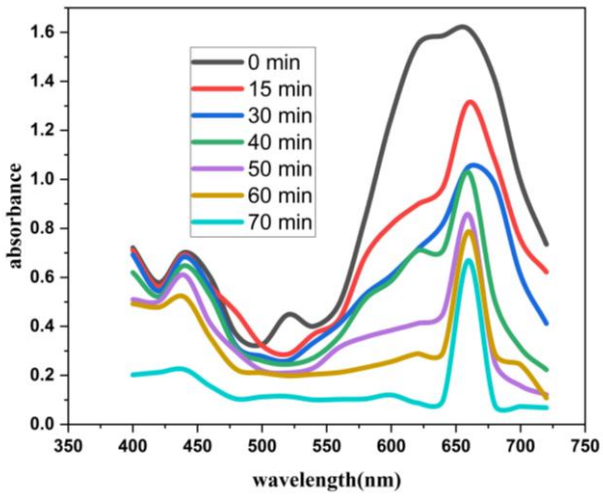

Figure 4: Absorbance spectra of Co-Fe2O4/WFS Composite

3.4.2. Effect of pH

In 100 mL of 10 mg/L of the starting concentration of MB dye and a dose of 0.5 g under visible light for 120 minutes, the impact of pH on methylene blue dye photocatalytic degradation was examined in the pH range of 3–11. The pH of the MB solution was changed using either 0.1 M HCl or 0.1 M NaOH. Additionally, the pH of the MB dye solution was measured both prior to and following the photocatalytic degradation process. Figure 5 shows that photocatalytic degradation was greatest at alkaline pH and least in acidic medium.

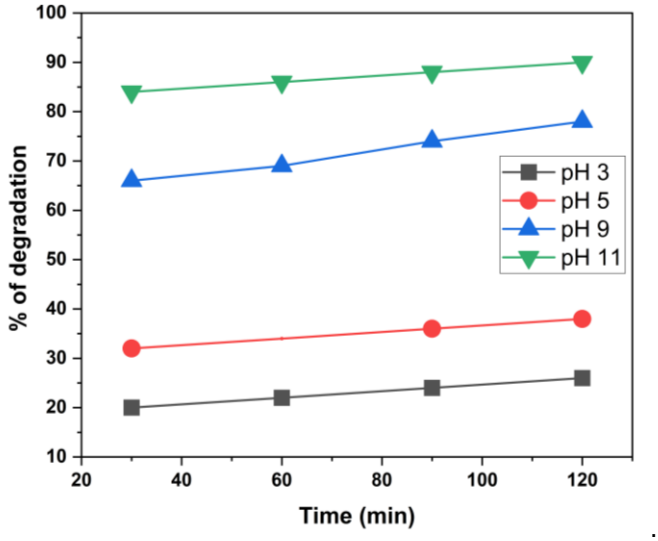

Figure 5: pH effect of $CoFe_2O_4$/WFS on MB dye

3.4.3. Effect of dose of catalyst

In this study Composite dosages ranged from 0.05 g to 0.4 g in order to assess the catalyst's role. In beakers with 100 mL of MB dye at a pH of 11 and a concentration of 10 mg/L, various concentrations of catalysts were added. A magnetic stirrer operating at 400 rpm was used to agitate the sample while it was in the photoreactor for 120 minutes. For different catalyst doses, a plot showing the percentage of methylene blue dye degradation vs time was created. It is evident from Figure 6 that the maximum deterioration occurred at a catalyst level of 0.3 g. The photocatalytic degradation of dye decreased as the catalyst dose was increased further.

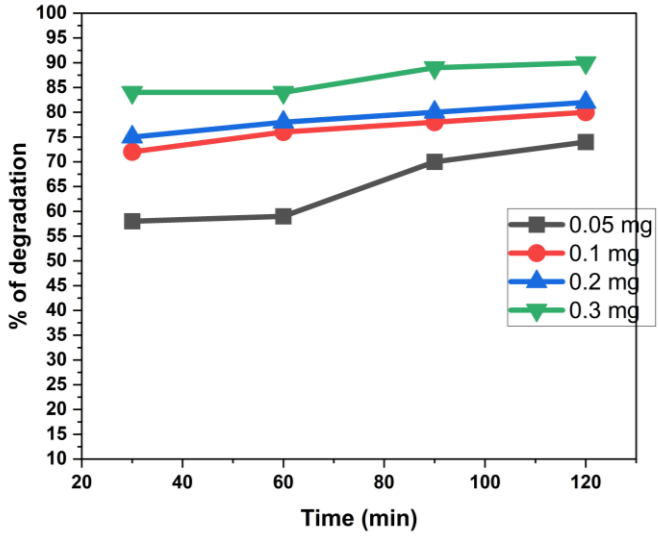

Figure 6: Mass dose effect of $CoFe_2O_4$/WFS on MB dye

3.4.4. Effect of initial concentration of MB dye solution

Using a fixed photocatalyst dose of 0.3 g at different beginning concentrations of MB dye ranging from 5 mg/L to 20 mg/L from a stock solution of 100 mg/L with pH 9 under visible light for 120 minutes, the impact of the initial concentration on the photodegradation process was investigated. The graph was then plotted as the percentage of degradation against time. As concentration rises, dye removal falls.

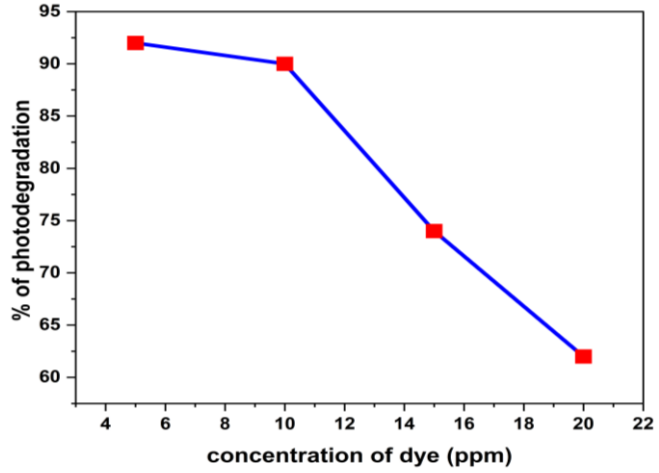

Figure 7: Initial Concentration of MB Dye Solution

3.4.5 Catalyst reusability

- Composite reused for **4 cycles** with <10% efficiency drop.

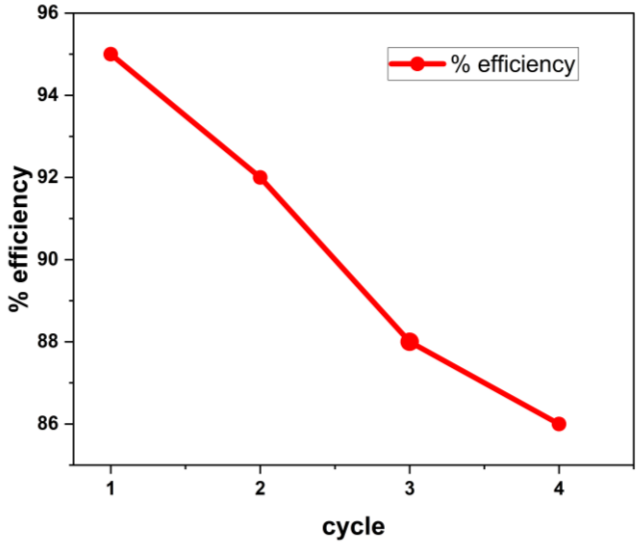

Figure 8: Recyclability Graph of $CoFe_2O_4$/WFS

Conclusion

The effective synthesis of a new Co-Fe_2O_4/WFS composite showed good photocatalytic efficiency toward the degradation of Methylene Blue under visible light. Important conclusions:

- Effective cooperation between photocatalysis ($CoFe_2O_4$) and adsorption (WFS)
- Reusable for up to many cycles and magnetically recoverable
- Economical, eco-friendly, and appropriate for industrial use.

References

1. Hussain, S., Khan, N., Gul, S., Khan, S., & Khan, H. (2020). Contamination of water resources by food dyes and its removal technologies. In *Water chemistry* (pp. 1–14). IntechOpen.
2. Berradi, M., Hsissou, R., Khudhair, M., Assouag, M., Cherkaoui, O., El Bachiri, A., & El Harfi, A. (2019). Textile finishing dyes and their impact on aquatic environs. *Heliyon, 5*, e02711.
3. Gičević, A., Hindija, L., & Karačić, A. (2020). Toxicity of azo dyes in pharmaceutical industry. In *CMBEBIH 2019: Proceedings of the International Conference on Medical and Biological Engineering* (pp. 581–587). Springer.
4. Singh, A. K., & Chandra, R. (2019). Pollutants released from the pulp paper industry: Aquatic toxicity and their health hazards. *Aquatic Toxicology, 211*, 202–216.
5. Lima, J., & Aguiar, A. (2021). Presença de metais pesados e processos convencionais para o tratamento de efluentes de indústrias têxteis brasileiras. In *Engenharia química: Inovação e tradição em tempos de pandemia* (pp. 806–819). Even3 Publicações.
6. Ramos, M. D. N., Lima, J. P. P., de Aquino, S. F., & Aguiar, A. (2021). A critical analysis of the alternative treatments applied to effluents from Brazilian textile industries. *Journal of Water Process Engineering, 43*, 102273.

7. Tkaczyk, A., Mitrowska, K., & Posyniak, A. (2020). Synthetic organic dyes as contaminants of the aquatic environment and their implications for ecosystems: A review. *Science of the Total Environment, 717*, 137222.
8. Garrido-Cardenas, J. A., Esteban-García, B., Agüera, A., Sánchez-Pérez, J. A., & Manzano-Agugliaro, F. (2020). Wastewater treatment by advanced oxidation processes and their worldwide research trends. *International Journal of Environmental Research and Public Health, 17*, 170.
9. Kowalska, K., Maniakova, G., Carotenuto, M., Sacco, O., Vaiano, V., Lofrano, G., & Rizzo, L. (2020). Removal of carbamazepine, diclofenac and trimethoprim by solar-driven advanced oxidation processes in a compound triangular collector-based reactor: A comparison between homogeneous and heterogeneous processes. *Chemosphere, 238*, 124665.
10. Akerdi, A. G., & Bahrami, S. H. (2019). Application of heterogeneous nano-semiconductors for photocatalytic advanced oxidation of organic compounds: A review. *Journal of Environmental Chemical Engineering, 7*, 103283.
11. Xie, X., Wang, B., Wang, Y., Ni, C., Sun, X., & Du, W. (2022). Spinel structured MFe_2O_4 (M = Fe, Co, Ni, Mn, Zn) and their composites for microwave absorption: A review. *Chemical Engineering Journal, 428*, 131160.
12. Sundararajan, M., Sailaja, V., John Kennedy, L., & Judith Vijaya, J. (2017). Photocatalytic degradation of rhodamine B under visible light using nanostructured zinc-doped cobalt ferrite: Kinetics and mechanism. *Ceramics International, 43*, 540–548.
13. Rashad, M. M., Mohamed, R. M., Ibrahim, M. A., Ismail, L. F. M., & Abdel-Aal, E. A. (2012). Magnetic and catalytic properties of cubic copper ferrite nanopowders synthesized from secondary resources. *Advanced Powder Technology, 23*, 315–323.
14. Sivakumar, P., Ramesh, R., Ramanand, A., Ponnusamy, S., & Muthamizhchelvan, C. (2011). Synthesis and characterization of nickel ferrite magnetic nanoparticles. *Materials Research Bulletin, 46*, 2208–2211.
15. Priya, R., Stanly, S., Anuradha, R., & Sagadevan, S. (2019). Evaluation of photocatalytic activity of copper ferrite nanoparticles. *Materials Research Express, 6*, 095014.
16. Karcıoğlu Karakaş, Z. (2022). A comprehensive study on the production and photocatalytic activity of copper ferrite nanoparticles synthesized by microwave-assisted combustion method as an effective photocatalyst. *Journal of Physics and Chemistry of Solids, 170*, 110927.
17. Vosoughifar, M. (2016). Preparation and application of copper ferrite nanoparticles for degradation of methyl orange. *Journal of Materials Science: Materials in Electronics, 27*, 10449–10454.
18. Oliveira, T. P., Rodrigues, S. F., Marques, G. N., Viana Costa, R. C., Garçone Lopes, C. G., Aranas, C., Rojas, A., Gomes Rangel, J. H., & Oliveira, M. M. (2022). Synthesis, characterization, and photocatalytic investigation of $CuFe_2O_4$ for the degradation of dyes under visible light. *Catalysts, 12*, 623.
19. Ismael, M. (2021). Ferrites as solar photocatalytic materials and their activities in solar energy conversion and environmental protection: A review. *Solar Energy Materials and Solar Cells, 219*, 110786.
20. Behera, A., Kandi, D., Majhi, S. M., Martha, S., & Parida, K. (2018). Facile synthesis of $ZnFe_2O_4$ photocatalysts for decolourization of organic dyes under solar irradiation. *Beilstein Journal of Nanotechnology, 9*, 436–446.

21. Jarusheh, H. S., Yusuf, A., Banat, F., Haija, M. A., & Palmisano, G. (2022). Integrated photocatalytic technologies in water treatment using ferrite nanoparticles. *Journal of Environmental Chemical Engineering, 10*, 108204.
22. Dhiwahar, A. T., Maruthamuthu, S., Marnadu, R., Sundararajan, M., Manthrammel, M. A., Shkir, M., Sakthivel, P., & Minnam Reddy, V. R. (2021). Improved photocatalytic degradation of rhodamine B under visible light and magnetic properties using microwave combustion-grown Ni-doped copper ferrite spinel nanoparticles. *Solid State Sciences, 113*, 106542.
23. Silva, M. M. S., Raimundo, R. A., Silva, T. R., Araújo, A. J. M., Macedo, D. A., Morales, M. A., Souza, C. P., Santos, A. G., & Lopes-Moriyama, A. L. (2023). Morphology-controlled $NiFe_2O_4$ nanostructures: Influence of calcination temperature on structural, magnetic and catalytic properties towards OER. *Journal of Electroanalytical Chemistry, 933*, 117277.
24. Nihore, A., Aziz, F., Oswal, N., Jain, P., Subohi, O., & Gupta, N. (2019). Synthesis and characterization of copper-doped nickel ferrite prepared by sol–gel method. *Materials Today: Proceedings, 18*, 3651–3656.
25. Anjana, V., John, S., Prakash, P., Nair, A. M., Nair, A. R., Sambhudevan, S., & Shankar, B. (2018). Magnetic properties of copper-doped nickel ferrite nanoparticles synthesized by co-precipitation method. *IOP Conference Series: Materials Science and Engineering, 310*, 012024.
26. Gayathri Manju, B., & Raji, P. (2019). Biological synthesis, characterization, and antibacterial activity of nickel-doped copper ferrite nanoparticles. *Applied Physics A, 125*, 313.
27. Greenwood, N. N. (2012). *Mössbauer spectroscopy*. Springer.
28. Silva, M. M. S., Raimundo, R. A., Ferreira, L. S., Macedo, D. A., Morales, M. A., Souza, C. P., Santos, A. G., & Lopes-Moriyama, A. L. (2022). Effects of morphology on the electrochemical performance of $NiFe_2O_4$ nanoparticles with battery-type behavior. *International Journal of Applied Ceramic Technology, 19*, 2016–2028.
29. Thanh, N. K., Loan, T. T., Anh, L. N., Duong, N. P., Soontaranon, S., Thammajak, N., & Hien, T. D. (2016). Cation distribution in $CuFe_2O_4$ nanoparticles: Effects of Ni doping on magnetic properties. *Journal of Applied Physics, 120*, 142115.